J. Plasma Physics (2012), *vol.* 78, *part* 4, *pp.* 327–331. © Cambridge University Press 2012
doi:10.1017/S0022377811000602

Forward directed ion acceleration in a LWFA with ionization-induced injection

N. LEMOS[1], J.L. MARTINS[1], J.M. DIAS[1], K.A. MARSH[2], A. PAK[3] and C. JOSHI[2]

[1]GoLP/Instituto de Plasmas e Fusão Nuclear – Laboratório Associado, Instituto Superior Técnico, Technical University of Lisbon, Av. Rovisco Pais, 1049-001 Lisbon, Portugal (nuno.lemos@ist.utl.pt)
[2]Department of Electrical Engineering, UCLA, Los Angeles, CA 90095, USA
[3]Livermore National Laboratory, 7000 East Ave., Livermore, CA 94550, USA

(Received 1 October 2011; revised 7 December 2011; accepted 12 December 2011; first published online 10 January 2012)

Abstract. In this work we present an experimental study where energetic ions were produced in an underdense 2.5×10^{19} cm^{-3} plasma created by a 50 fs Ti:Sapphire laser with 5 TWs of power. The plasma comprises 95% He and 5% N_2 gases. Ionization-induced trapping of nitrogen K-shell electrons in the laser-induced wakefield generates an electron beam with a mean energy of 40 MeV and ~1 nC of charge. Some of the helium ions at the wake–vacuum interface are accelerated with a measured minimum ion energy of He^{1+} ions of 1.2 MeV and He^{2+} ions of 4 MeV. The physics of the interaction is studied with 2D particle-in-cell simulations. These reveal the formation of an ion filament on the axis of the plasma due to space charge attraction of the wakefield-accelerated high-charge electron bunch. Some of these high-energy electrons escape the plasma to form a sheath at the plasma–vacuum boundary that accelerates some of the ions in the filament in the forward direction. Electrons with energy less than the sheath potential cannot escape and return to the plasma boundary in a vortex-like motion. This in turn produces a time-varying azimuthal magnetic field, which generates a longitudinal electric field at the interface that further accelerates and collimates the ions.

1. Introduction

The interaction of short-pulse high-intensity lasers with plasmas can generate energetic particles such as multi-MeV ions and GeV energy electrons. Typically, ion acceleration experiments are carried out using overdense plasmas (solid targets or clusters) where different acceleration mechanisms are possible: coulomb explosion (CE) [1], radiation pressure (RP) [2], target normal sheath acceleration (TNSA) [3] and some other mechanisms [4–6]. In all the first three mechanisms, plasma electrons are heated/accelerated by the laser pulse dragging the plasma ions with them because of the space charge force. In an underdense plasma, electrons can be accelerated by the generation of a relativistically propagating wake. As these electrons eventually leave the plasma, a longitudinal, quasi-DC electric field can be generated at the boundary between the wake (plasma) and the vacuum, which in turn will accelerate ions. Although ion acceleration with solid targets has been under intense study in the past decade, there is relatively little work on energetic ion generation due to wakefied acceleration of electrons. It is the intent of this work to explore this problem. There has been some previous work on ion acceleration in underdense plasmas. In Krushelnick et al. [7], for instance, Ne ions with energy of up to 6 MeV were seen in the radial direction to the intense laser pulse and interpreted as being accelerated by the impulse imparted by the expelled plasma electrons. In Willingale et al. [8] and Bulanov and Esirkepov [9], ions were accelerated longitudinally in an underdense plasma up to 40-MeV energy using a 1-ps long Petawatt (PW) class laser pulse with an a_0 of 21. In computer simulations, it is seen that in this later case the accelerated electrons set up a longitudinal electrical field at the plasma–vacuum boundary. As the highest energy electrons leave the plasma, they create a charge separation or a sheath. The lower energy electrons however are pulled back into the plasma in a vortex-like motion capable of producing an azimuthal quasi-static magnetic field at the interface [9, 10–13]. This time-dependent B field in turn produces an additional electric field capable of accelerating and collimating the ions. Both of these effects can then accelerate a thin layer of ions to several megaelectron volts (MeV) of energy. We show here through experiments that this forward (longitudinal) ion emission also occurs in very dilute plasmas even when using a more modest few TW class laser where the electrons are accelerated by the wakefield and not by direct laser acceleration. In order to get the additional contribution from the magnetic field to ion acceleration, it is necessary to have the wake terminate at the plasma–vacuum boundary and a hot and high-charge electron beam must be ejected from the

https://doi.org/10.1017/S0022377811000602 Published online by Cambridge University Press

plasma. We find that although the self-injection mechanism in laser wakefield acceleration (LWFA) generates electron beams that typically contain tens of pC of charge, the charge is too low to produce a significant number of ions. Recent experiments have shown that ionization-induced trapping [14, 15] in a laser-induced wake can accelerate nC of charge, albeit with a continuous energy spread, with a mean energy of ten hundreds of MeV with a relatively high temperature (~5 MeV) in an underdense plasma. In this work we show that by employing ionization-induced trapping, such high-charge electron beams can indeed be generated and these in turn can produce several MeV energy He^{2+} ions in an underdense 2.5×10^{19} cm^{-3} plasma using a Ti:Sapphire laser with 5 TWs of power. The mechanism of ion acceleration is revealed in 2D particle-in-cell (PIC) computer simulations using the code OSIRIS [16]. These show that the longitudinal electric field created by the azimuthal quasi-static magnetic field contributes predominantly to the acceleration of ions in our case.

2. Experimental setup

Experiments were conducted at UCLA using a Ti:Sapphire laser (central wavelength of 815 nm) with laser pulse energy of ⩽340 mJ on target and an average pulse width of 50 fs (FWHM). A schematic of the experimental setup is shown in Fig. 1(a). The laser pulse was focused 100 μm inside a 1-mm wide column of gas created by a supersonic nozzle. The vacuum spot size w_0 was 6 μm at the $1/e^2$ intensity point. The peak intensity was 10^{19} W/cm^2 and the normalized vector potential a0 of the laser pulse was 2.3. Interferometer measurements indicate that the typical plasma electron density profile consisted of a 250-μm density up-ramp followed by a 500-μm plateau with a density $ne = 2.5 \times 10^{19}$ cm^{-3} and then a 250-μm density down ramp. In previous experiments we have shown that the addition of a small amount of nitrogen to the predominantly helium plasma leads to the ionization trapping and acceleration of K-shell electrons of nitrogen in a wake that is predominantly sustained by helium electrons. Continuous injection of these K-shell electrons leads to a broad energy spread spectrum. In the present experiments we use a gas mix of 95% He and 5% N_2 in order to increase the accelerated charge and thereby improve the chance of observing the forward ion emission. The generated electron beams were dispersed in the plane of laser polarization onto a LANEX screen, placed 18.5 cm from a dipole magnet with a magnetic field of 1 T extending over 6.5 cm. The ions were detected with a stack of solid-state track detectors. The detectors consisted of two 1-mm thick CR39 plates with an area of 50 × 50 mm (see Fig. 1(b) and (c)). The electrons represented in blue go through the dipole magnet bending to the left and the ions represented in green bend to the right (as shown in Fig. 1(b)). The CR39 plates are off-axes relative to the laser axes so that the

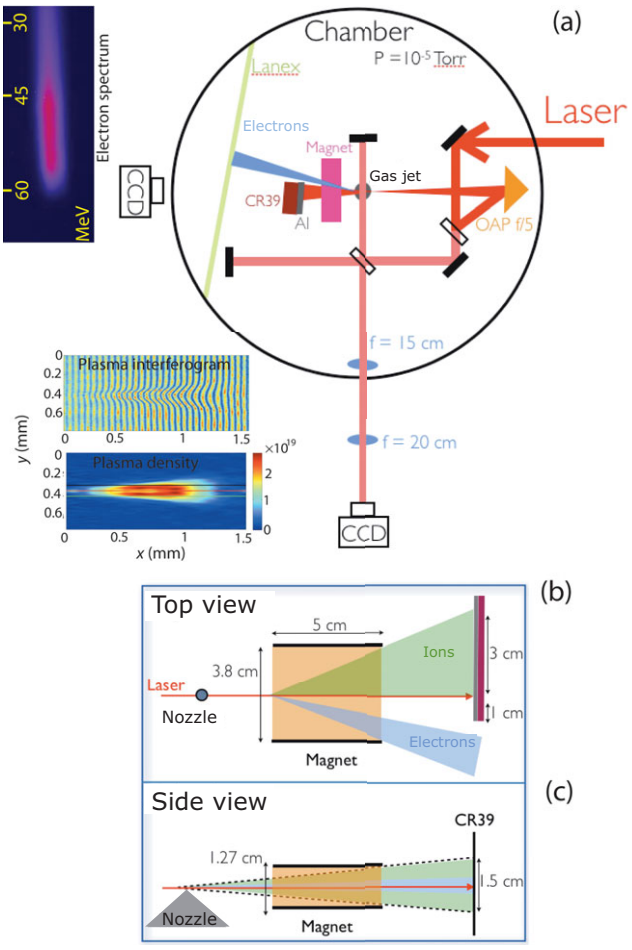


Figure 1. (Colour online) (a) Schematic of the experimental setup showing online interferometer and electron spectrometer; (b) diagram of the top view of the setup; (c) diagram of the side view of the setup.

deflected electron beam does not hit them. Also, a single 12-μm aluminium foil was placed in front of the CR39 plates to protect them from possible damage induced by the transmitted portion of the main laser beam. After exposure to ions, the CR39 plates were etched in a six molar NaOH solution for 6 h so that pits are formed in the regions damaged by ions. The pits on these plates were analyzed and counted using an automated software combined with a microscope.

3. Experimental results

As stated earlier, two types of gases were used, pure He and a gas mix of 95% He and 5% N_2. After processing the CR39 plates for these two different gases we saw that in the case of pure helium, the plates did not show any pits above the background level but when using the gas mix, there were pits evidence for multi-MeV helium ions in the plates.

Figures 2(a) and (b) show images of the etched pits from two back-to-back CR39 plates when using the

https://doi.org/10.1017/S0022377811000602 Published online by Cambridge University Press

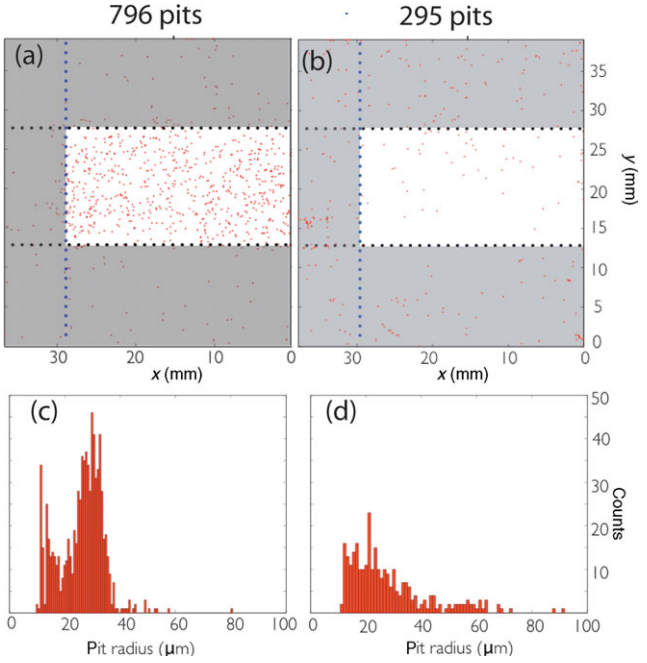


Figure 2. (Colour online) (a) Pits created by the accelerated ions on the first CR39 plate, where the grey part represents the shadow of the electron spectrometer (magnet); (b) pits on the second CR39 plate; (c) pit size distribution on the first CR39 plate; (d) pit size distribution on the second CR39 plate.

He/N gas mix to form the plasma. These images are obtained after firing five laser shots, where each red dot represents a single ion pit. The grey region represents the expected shadow created by the dipole magnet (5-cm iron thick), providing the noise level of the CR39 sheet. It is clear from this figure that the ions were stopped at the front surface of the first plate of CR39. The second plate (Fig. 2(b)) had no signal because the pit concentration is at the noise level. The noise pit concentration is 20 pits cm^{-2} and the pit concentration of the real signal (outside the grey region in the first plate) is 90 pits cm^{-2}, well above the noise. Figures 2(c) and (d) show the plots of the pit size distribution. It is possible to see that the difference between these two images is the spike located around 30 μm, indicating that these are the pits corresponding to real signal (outside the grey part). We also made simultaneous measurements of electrons that escaped the plasma. As shown in Fig. 1(a), the measured electron beams had a continuous energy spectrum of up to 70 MeV, with a mean energy of 40 MeV and a total charge (including the low energy part) of up to 1 nC at a measured plasma density $\sim 2.5 \times 10^{19}$ cm^{-3}. The energy range of the ions is determined quantitatively from the tracks recorded in the CR39 plates by calculating their stopping ranges. Since the gas target is a mixture of 95% He and 5%N_2, highly charged ions of helium and nitrogen are the possible candidates for the accelerated ions. As helium ions and electrons constitute most of the plasma, we expect that the observed pits are mostly from He^{1+} and He^{2+}. The 12 μm aluminium foil that was in front of the CR39 plates blocks ions of He^{1+} with energy

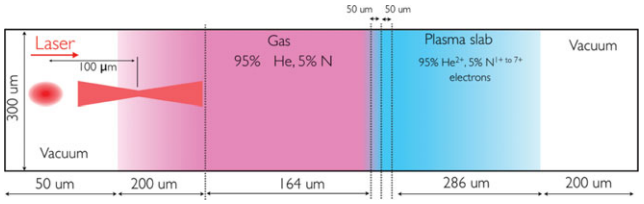


Figure 3. (Colour online) Layout of the 2D pic simulation with a box of 1000 × 300 μm with a resolution of 28.5 cells/λ in the longitudinal direction and 5.4 cells/λ in the transverse direction.

lower than 1.2 MeV and He^{2+} with energy lower than 4 MeV. Analyzing both plates of CR39 we only observed ion tracks on the front surface of the first sheet of CR39 (Fig. 2(a)). The second sheet and indeed the rear surface of the first sheet had very few pits that were within the noise range. The energy resolution of this measurement is directly dependent on the thickness of the CR39 sheet. This way assuming that all the ions were stopped within the first sheet of CR39, the possible energy range for He^{1+} ions is from 1.2 to 17.5 MeV and for He^{2+} ions, it is from 4 to 40 MeV. As for the measured charge, considering that most of the measured ions were He^{2+}, the number of accelerated ions with energy over 4 MeV (aluminium foil blocks ions with lower energy) was 796 that corresponds to the number of measured pits in the first CR39 plate. This number corresponds to an accumulation of five laser shots, so 159 ions/pits where produced for each laser shot (10^{-5} pC).

4. Simulations

Previous experiments and simulations [14, 17] have shown that at this plasma density and laser intensity the laser pulse can excite a wakefield in the so-called blowout regime where the laser pulse intensity is sufficiently large to blow out most of the plasma electrons that are subsequently attracted by the relatively immobile ions to excite a wakefield. The code OSIRIS 2.0 [16] was used to study the mechanism of ion acceleration at the plasma–vacuum boundary in this blowout regime. The simulations were done using a stationary simulation box in order to observe the plasma–vacuum boundary region after the laser has passed. The box was 1000 × 300 μm with a resolution of 28.5 cells/λ in the longitudinal direction and 5.4 cells/λ in the transverse direction.

Figure 3 shows the layout of a typical 2D simulation. The laser is launched from the left-hand side of the simulation box in a 50 μm vacuum region. This is followed by a region filled with gas that has a 200 μm density up ramp and a 164 μm region of constant density. Since we wanted to track ions at the plasma–vacuum boundary, we created a plasma region after the gas region. This region consists of a 50 μm density up ramp that is overlapped with the density down ramp of the gas region, in order to make a smooth transition, followed by a 50 μm region of constant density and a 286 μm density down ramp. The plasma constituted of

https://doi.org/10.1017/S0022377811000602 Published online by Cambridge University Press

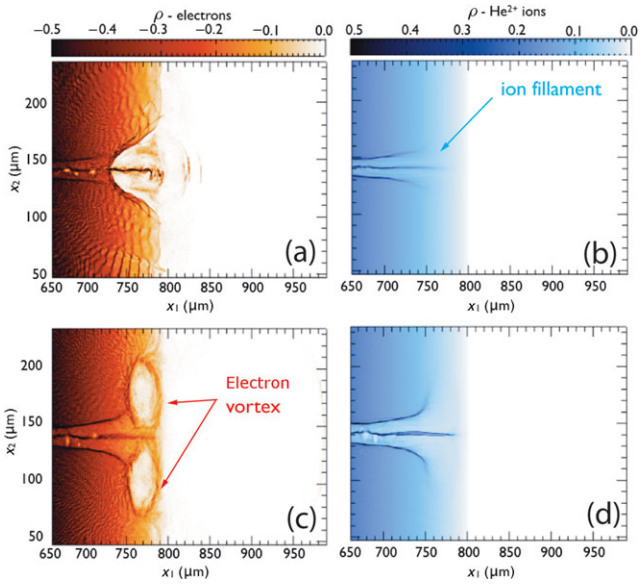


Figure 4. (Colour online) Charge density of electrons when the laser crossed the plasma–vacuum boundary; (b) charge density of He^{2+} ions when the laser crossed the plasma–vacuum boundary; (c) charge density of the electrons 0.83 ps after the laser crossed the plasma–vacuum boundary; (d) charge density of the ions 0.83 ps after the laser crossed the plasma–vacuum boundary.

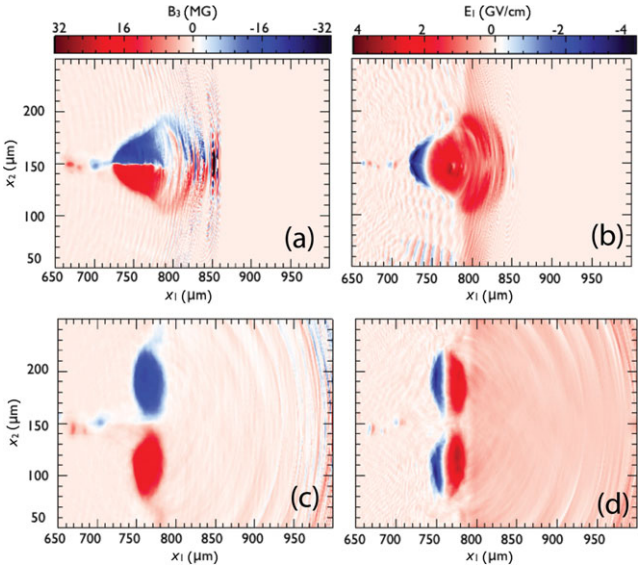


Figure 5. (Colour online) Bz magnetic field when the laser crossed the plasma–vacuum boundary; (b) Ex longitudinal electric field when the laser crossed the plasma–vacuum boundary; (c) Bz magnetic field 0.83 ps after the laser crossed the plasma–vacuum boundary; (d) Ex longitudinal electric field 0.83 ps after the laser crossed the plasma–vacuum boundary.

2.5×10^{19} cm^{-3} electrons, 9.1×10^{18} cm^{-3} He^{2+} and 9.65×10^{17} cm^{-3} N^{5+} ions. In the center we added a slab of plasma that contained 9.65×10^{17} cm^{-3} N^{7+} ions. This was made to simulate the center part where the laser pulse can fully ionize Nitrogen. The vacuum then extended further by 200 μm behind the plasma. The laser pulse was linearly polarized (in plane of the simulation) with a pulse duration of 50 fs and a wavelength of 815 nm. It was focused in the middle of the left density ramp with a spot size of 5.9 μm (full width at half maximum (FWHM) of the electric field) with a peak normalized vector potential $a0 = 3$. As the laser propagates in the plasma, the ponderomotive force of the laser expels electrons from the laser axis leaving a cavitated region, referred to as the blowout region [18]. This region follows the laser with a phase velocity equal to the group velocity of the laser while the ions remain at rest (in the time scale of the laser) behind the laser pulse. The trapped electrons (either through self-trapping [18, 19] or ionization trapping [14]) are bunched in the center of the blowout region where they create a very strong electrostatic field due to very high charge density of the bunch. This field then acts on the ions and radially accelerates them inwards as discussed by Popov et al. [20].

The ions start to move toward the axis and later form a density filament on axis as shown in Fig. 4(b). The rest of the ions inside the blowout region but outside the electron bunch region are accelerated away from the axis due to the repulsive force between them. When the laser crosses the plasma–vacuum boundary, it leaves behind the blowout region that is positively charged (Fig. 4(a)) with a narrow central filament of ions (Fig. 4(b)) and electrons (Fig. 4(a)).

When the electron bunch gets to the plasma–vacuum boundary, the most energetic electrons escape the plasma (Fig. 4(a)), setting up a plasma potential barrier. This in turn confines the lower energy electrons. As these electrons are pulled back into the plasma (return current), they form a vortex [11, 12] (Fig. 4(c)) with an accompanying magnetic field that can reach tens of megagauss in magnitude (Fig. 5(c)). By Faraday's law, this magnetic field in turn produces a longitudinal electric field. This slowly varying longitudinal accelerating electric field can reach tens of GV/m (Fig. 5(d)). In this scenario the B field has a defocusing effect that is negligible compared to the focusing force generated by the electric field. In this manner the ion filament is maintained (Fig. 4(d)) until the magnetic field decays over time. In our simulation the magnetic field is maintained for 1.32 ps (remember that the plasma oscillation period is just ∼20 fs) after the laser crossed the plasma–vacuum boundary.

The energy that the ions gain until 1.32 ps is 3.7 MeV (Fig. 6(a)). After this time the acceleration continues, but at a slower rate where the dominant acceleration mechanism is TNSA. After 4.73 ps (or 2.43 ps after the dissipation of magnetic field) the ion energy is about 6.2 MeV (Fig. 6(b)), meaning that the TNSA fields accelerate ions at roughly one-third the rate of the longitudinal field arising from the B field. This simulation was repeated with a helium plasma. The same electron vortices were observed but with a lower associated magnetic field and lower longitudinal accelerating electric field. So the ion energy of 1.32 ps after the laser crossed the plasma–vacuum boundary was 2 MeV,

https://doi.org/10.1017/S0022377811000602 Published online by Cambridge University Press

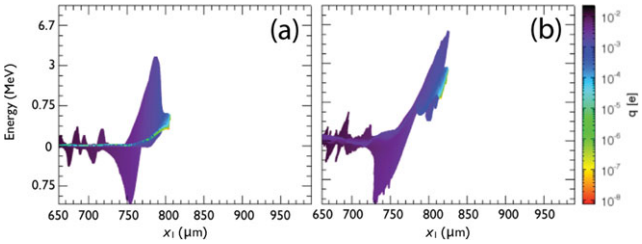


Figure 6. (Colour online) Longitudinal energy of the ion filament 1.32 ps after the laser crossed the plasma–vacuum boundary with a maximum energy of 3.7 MeV; (b) longitudinal energy of the ion filament 4.06 ps after the laser crossed the plasma–vacuum boundary with a maximum energy of 6.2 MeV.

almost half of the case when using the 95% He and 5% N gas mix. In this case there is a factor of ∼50% reduction in the trapped charge, which then results in weaker vortices and weaker induced longitudinal electric field. After the magnetic field induced by these vortices has dissipated, the dominant acceleration mechanism once again was TNSA and the ion energy was about 3.1 MeV (4.06 ps after the laser crossed the plasma–vacuum boundary). Recall that in the experiment no ions where observed when a pure helium plasma was used. As for the accelerated ion charge in the simulations, the measured charge was in the pC range for both simulations (gas mix and 100% He). The measured charge only corresponds to the ions that are in the central filament. The smaller charge measured in the experiment can possibly have two explanations: first, by the partial blocking of the ion beam by the magnet; second, it is known that 2D simulations often generate more charge than 3D simulations. In a future publication we will address this problem in a more profound way comparing 2D with 3D simulations.

5. Conclusions

We have studied the acceleration of ions at the plasma–vacuum boundary in the blowout regime. We have experimentally measured ions with a He/N_2 gas mix with a lower bound on the ion energy of 1.2 (He^{1+}) – 4 (He^{2+}) MeV when irradiating the gas jet target with a 5-TW laser. Simulations showed that an ion filament is formed on the axis of the plasma due to space charge attraction of high charge of the accelerated electron bunch. Some of the ions from this ion filament are then accelerated to MeV of energy by a longitudinal electric field created by the time-varying magnetic field due to the return current of the lower energy electrons.

Acknowledgments

The work of NRCL was partially supported by FCT Portugal through the grants SFRH/BD/37838/2007 and SFRH/BD/39523/2007, and DOE grant DE-FG02-92-ER40727 and NSF grant PHY-0936266 at UCLA. The authors would like to thank Dr. T. Grismayer and Professor W. Mori for fruitful discussions. The authors would also like to thank the Osiris consortium (UCLA/IST) for the use of Osiris.

References

[1] Bulanov, S. V., Esirkepov, T. Zh, Khoroshkov, V. S., Kuznetsov, A. V. and Pegoraro, F. 2002 *Phys. Lett.* A **299**, 240.
[2] Esirkepov, T., Borghesi, M., Bulanov, S. V., Moutou, G. and Tajima, T. 2004 *Phys. Rev. Lett.* **92**, 175003.
[3] Wilks, S. C., Langdon, A. B., Cowan, T. E., Roth, M., Singh, M., Hatchett, S., Key, M. H., Pennington, D., MacKinnon, A. and Snavely, R. A. 2001 *Phys. Plasmas* **8**, 542.
[4] Fuchs, J. et al. 2006 *Nature Phys.* **2**, 48–54.
[5] Denavit, J., 1992 *Phys. Rev. Lett.* **69**, 3052.
[6] Silva, L. O. et al. 2004 *Phys. Rev. Lett.* **92**, 015002.
[7] Krushelnick, K. et al. 1999 *Phys. Rev. Lett.* **83**(4), 737–740.
[8] Willingale, L. et al. 2006 *Phys. Rev. Lett.* **96**(24), 245002.
[9] Bulanov, S. V. and Esirkepov, T. Zh., 2007 *Phys. Rev. Lett.* **98**, 049503.
[10] Kolodner, P. et al. 1979 *Phys. Rev. Lett.* **43**, 1402.
[11] Bulanov, S . V. et al. 2000 *Phys. Rev. Lett.* **71**, 407.
[12] Bulanov, S. V. et al. 2005 *Plasma Phys. Rep.* **31**(5), 369–381.
[13] Fukuda, Y. et al. 2009 *Phys. Rev. Lett.* **103**(16), 165002.
[14] Pak, A. et al. 2010 *Phys. Rev. Lett.* **104**(2), 025003.
[15] Clayton, C. E. et al. 2010 *Phys. Rev. Lett.* **105**(10), 105003.
[16] Fonseca, R. A. et al. 2002 *Lect. Notes Comput. Sci.* **2331**, 342; Fonseca, R. A., Martins, S. F., Silva, L. O., Tonge, J. W., Tsung, F. and Mori, W. B. 2008 *Plasma Phys. Control. Fusion* **50**, 124034.
[17] Ralph, J. E. et al. 2009 *Phys. Rev. Lett.* **102**, 175003.
[18] Lu, W. et al. 2007 *Phys. Rev. Spec. Top. – Accelerators and Beams* **10**, 061301.
[19] Kostyukov, E. et al. 2009 *Phys. Rev. Lett.* **103**(17), 175003.
[20] Popov, K. I. et al. 2010 *Phys. Rev. Lett.* **105**(19), 195002.

https://doi.org/10.1017/S0022377811000602 Published online by Cambridge University Press